Research Square

Preprints are preliminary reports that have not undergone peer review.
They should not be considered conclusive, used to inform clinical practice,
or referenced by the media as validated information.

Revisiting Diurnal Variation Correction for Regional Total-Field Magnetic Surveys: Accounting for the DI Effect

Seitaro Ono

seitaro.ono@aist.go.jp

AIST: Kokuritsu Kenkyu Kaihatsu Hojin Sangyo Gijutsu Sogo Kenkyujo https://orcid.org/0009-0002-4555-7462

Taichi Sato

AIST: Kokuritsu Kenkyu Kaihatsu Hojin Sangyo Gijutsu Sogo Kenkyujo

Hiroaki Koge

AIST: Kokuritsu Kenkyu Kaihatsu Hojin Sangyo Gijutsu Sogo Kenkyujo

Seiki Asari

Kakioka Magnetic Observatory

Shingo Nagamachi

Kakioka Magnetic Observatory

Research Article

Keywords: Diurnal variation correction, Total-field magnetic survey, DI effect, Crossover difference

Posted Date: October 26th, 2026

DOI: https://doi.org/10.21203/rs.3.rs-11246967/v1

License: This work is licensed under a Creative Commons Attribution 4.0 International License.
Read Full License

Revisiting Diurnal Variation Correction for Regional Total-Field Magnetic Surveys: Accounting for the DI Effect

Author #1: Seitaro Ono, Geological Survey of Japan, National Institute of Advanced Industrial Science and Technology (AIST), 1-1-1 Higashi, Tsukuba, Ibaraki 305-8567, Japan, seitaro.ono@aist.go.jp

Author #2: Taichi Sato, Geological Survey of Japan, National Institute of Advanced Industrial Science and Technology (AIST), 1-1-1 Higashi, Tsukuba, Ibaraki 305-8567, Japan, taichi-sato@aist.go.jp

Author #3: Hiroaki Koge, Geological Survey of Japan, National Institute of Advanced Industrial Science and Technology (AIST), 1-1-1 Higashi, Tsukuba, Ibaraki 305-8567, Japan, koge.h@aist.go.jp

Author #4: Seiki Asari, Kakioka Magnetic Observatory, Japan Meteorological Agency, Kakioka 595, Ishioka, 315-0116, Japan, s.asari@met.kishou.go.jp

Author #5: Shingo Nagamachi, Kakioka Magnetic Observatory, Japan Meteorological Agency, Kakioka 595, Ishioka, 315-0116, Japan, nagamachi@met.kishou.go.jp

corresponding author: Seitaro Ono (seitaro.ono@aist.go.jp)

Abstract

Diurnal variation correction is essential for obtaining reliable total-field magnetic anomalies in regional marine and airborne magnetic surveys. Conventional correction methods directly subtract the total-field variation recorded at a reference geomagnetic observatory from the survey data. However, total-field variations represent projections of vector magnetic-field variations onto the local geomagnetic-field direction. Differences in declination and inclination between the reference observatory and survey area can therefore leave residual external-field variations, referred to as the "DI effect". In this study, we systematically compared three methods for correcting diurnal variations in regional moving-platform total-field magnetic surveys: conventional diurnal variation correction (CDV correction), least-squares DI correction originally developed for stationary observations (LS-DI correction), and IGRF-based DI correction (IGRF-DI correction). The IGRF-DI correction projects vector magnetic-field variations recorded at a reference observatory onto the local direction of the International Geomagnetic Reference Field at each survey location and observation time, without requiring empirical estimation of correction coefficients from the survey

data. The three methods were evaluated using total-field magnetic data acquired during two marine surveys and vector magnetic-field data from four geomagnetic observatories distributed over a wide latitudinal range. Correction performance was quantified using the root mean square (RMS) of crossover differences. For both surveys and all four reference observatories, the IGRF-DI correction produced lower crossover RMS values than the conventional correction, with greater improvements generally observed for larger angular differences in main-field direction, where the DI effect is expected to be more pronounced. The performance of the LS-DI correction varied substantially among reference observatories. Although it occasionally produced low crossover RMS values, its estimated coefficients differed markedly from those predicted from the IGRF. These results suggest that least-squares estimation is fundamentally unsuitable for moving-platform surveys because spatial variation of crustal magnetic anomalies can be misinterpreted as temporal external-field variations. Overall, the comparison demonstrates that accounting for the DI effect improves diurnal variation correction in regional moving-platform surveys, whereas empirical least-squares estimation may produce physically unreliable corrections. We therefore recommend applying the IGRF-

DI correction using vector magnetic-field data from the nearest suitable geomagnetic observatory as a practical default strategy for regional total-field magnetic surveys.

Keywords

Diurnal variation correction, Total-field magnetic survey, DI effect, Crossover difference

1 Introduction

Geomagnetic surveys provide important information on crustal structure and tectonic processes and are widely conducted on the ground, at sea, and from the air. Total-field magnetic measurements contain contributions not only from crustal magnetic anomalies but also from the geomagnetic main field and external magnetic fields generated by ionospheric and magnetospheric current systems. Appropriate correction of these non-crustal components is therefore essential for reliable geological and geophysical interpretation.

One of the most fundamental processing steps in magnetic surveys is diurnal variation correction. This correction is commonly performed by subtracting temporal variations recorded at a reference geomagnetic observatory from survey observations (e.g., Sergipe et al., 2021). Such an approach implicitly assumes that total-field magnetic variations recorded at the observatory are identical to those observed within the survey area. However, total-field magnetic variations represent projections of vector magnetic-field variations onto the local geomagnetic field direction. Consequently, when the direction of the geomagnetic field differs between the reference observatory and the survey area, direct subtraction leaves residual external-field signals in the corrected data. This phenomenon has been referred to as the "orientation effect" (Davis and Johnston, 1983) or "DI effect" (e.g., Takahashi et al., 2018); hereafter, we use the term "DI effect". The DI effect becomes increasingly important as the angular difference in geomagnetic field direction increases.

To account for the DI effect, several studies have proposed correction methods that explicitly consider vector magnetic-field variations and differences in geomagnetic field direction (Sasai and Ishikawa, 1976; Tanaka et al., 1978; Davis et al., 1979). These

methods estimate correction coefficients from magnetic observations using a least-squares framework and have been successfully applied to stationary observations such as volcano-monitoring studies. In such applications, the observation site remains stationary and temporal magnetic-field variations can be separated relatively easily from local crustal magnetic anomalies. The applicability of these approaches to regional moving-platform surveys, however, has not been investigated. In shipborne, airborne, and other regional magnetic surveys, observation platforms move through areas where crustal magnetic anomalies vary spatially.

In this study, we compare and evaluate three different methods using total-field magnetic data acquired during two marine surveys together with vector magnetic-field data from four geomagnetic observatories distributed over a wide range in Japan. Correction performance is quantitatively evaluated using crossover root mean square (RMS) differences. We additionally investigate the physical validity of the least-squares coefficients and examine the relationship between correction performance and angular differences in geomagnetic field direction between the survey area and the reference observatory. Based on these results, we propose the most suitable way for diurnal

variation correction in regional total-field magnetic surveys. Our method will be standard diurnal variation correction method, leading to more precise geological interpretation.

2 Theory

2.1 Formulation of Total-Field Magnetic Anomalies and Variations

The total magnetic intensity $T_{obs}(t, \mathbf{x})$ observed at position $\mathbf{x}$ and time t is assumed to consist of the geomagnetic main field, crustal magnetic field, and external magnetic field diurnal variations:

$$T_{obs}(t, \mathbf{x}) = \|\mathbf{B_m}(t, \mathbf{x}) + \mathbf{B_c}(\mathbf{x}) + \mathbf{B_{dv}}(t)\|$$

where $\mathbf{B_m}(t, \mathbf{x})$ is the geomagnetic main field vector, $\mathbf{B_c}(\mathbf{x})$ is the crustal magnetic field vector, and $\mathbf{B_{dv}}(t)$ is the external magnetic field variation vector. $\mathbf{B_c}(\mathbf{x})$ is assumed to be time independent, while $\mathbf{B_{dv}}(t)$ is assumed to be spatially uniform. $\|\cdot\|$ denotes the vector norm.

The total-field magnetic anomaly $T_{anm}(t, \mathbf{x})$ is defined as

$$T_{anm}(t, \mathbf{x}) = T_{obs}(t, \mathbf{x}) - \|\mathbf{B_m}(t, \mathbf{x})\|.$$

Assuming

$$\|\mathbf{B_c}(\mathbf{x}) + \mathbf{B_{dv}}(t)\| \ll \|\mathbf{B_m}(t, \mathbf{x})\|$$

and performing a Taylor expansion, with second- and higher-order terms neglected,

$$T_{anm}(t, \mathbf{x}) = \|\mathbf{B_m}(t, \mathbf{x}) + \mathbf{B_c}(\mathbf{x}) + \mathbf{B_{dv}}(t)\| - \|\mathbf{B_m}(t, \mathbf{x})\|$$

$$\approx \widehat{\mathbf{B}}_\mathbf{m}(t, \mathbf{x}) \cdot \left(\mathbf{B_c}(\mathbf{x}) + \mathbf{B_{dv}}(t)\right) \quad (1)$$

where $\widehat{\mathbf{B}}_\mathbf{m}(t, \mathbf{x})$ denotes the unit vector of $\mathbf{B_m}(t, \mathbf{x})$ and the dot represents the inner product. Eq. (1) shows that total-field magnetic anomalies correspond to the projection of vector magnetic anomaly onto the local geomagnetic main field direction.

At a reference geomagnetic observatory, crustal magnetic anomalies can be regarded as constant and are removed when calculating magnetic field variations. Therefore, the total magnetic intensity observed at a reference station at time t, $T_{ref}(t)$, is expressed as

$$T_{ref}(t) = \|\mathbf{B_{base}} + \mathbf{B_{dv}}(t)\|$$

where $\mathbf{B_{base}}$ is the constant background magnetic field vector at the reference station. The total magnetic field variation observed at the reference station, denoted by $T_{dv}(t)$, can be derived by assuming

$$\|\mathbf{B_{dv}}(t)\| \ll \|\mathbf{B_{base}}\|,$$

and performing a Taylor expansion, with second- and higher-order terms neglected:

130 $$T_{dv}(t) = T_{ref}(t) - T_{base}$$

131 $$= \|\mathbf{B_{base}} + \mathbf{B_{dv}}(t)\| - \|\mathbf{B_{base}}\|$$

$$\approx \widehat{\mathbf{B}}_{\mathbf{base}} \cdot \mathbf{B_{dv}}(t) \quad (2)$$

132 where $\widehat{\mathbf{B}}_{\mathbf{base}}$ denotes the unit vector of $\mathbf{B_{base}}$.

133

134 **2.2 Conventional Diurnal Variation Correction (CDV Correction)**

135 Conventional diurnal variation correction (hereafter referred to as "CDV correction")

136 simply subtracts the total magnetic field variation observed at a reference station from

137 the magnetic field data measured at the survey location (e.g., Sergipe et al., 2021) and

138 this is very common correction method for regional survey. By subtracting Eq. (2) from

139 Eq. (1), the following expression is obtained:

$$T_{anm}(t, \mathbf{x}) - T_{dv}(t) \approx \widehat{\mathbf{B}}_{\mathbf{m}}(t, \mathbf{x}) \cdot \mathbf{B_c}(\mathbf{x}) + \left(\widehat{\mathbf{B}}_{\mathbf{m}}(t, \mathbf{x}) - \widehat{\mathbf{B}}_{\mathbf{base}}\right) \cdot \mathbf{B_{dv}}(t) \quad (3)$$

140 However, as evident from Eq. (1), accurate correction for diurnal variations in total-

141 field magnetic anomalies requires the removal of the term $\widehat{\mathbf{B}}_{\mathbf{m}}(t, \mathbf{x}) \cdot \mathbf{B_{dv}}(t)$. In

142 practice, most studies instead subtract the total magnetic field variation observed at the

143 reference station, i.e., $T_{dv}(t)$. Consequently, the apparent difference caused by called

144 "DI effect" remains in the corrected data. The discrepancy arising from the DI effect

145 can be expressed as

146 $$\left(\widehat{\mathbf{B}}_{\mathbf{m}}(t,\mathbf{x}) - \widehat{\mathbf{B}}_{\mathbf{base}}\right) \cdot \mathbf{B}_{\mathbf{dv}}(t)$$

147 where the discrepancy is proportional to the difference between the unit direction

148 vectors at the survey location and the reference station. Therefore, the effect becomes

149 more significant when the survey area is located far from the reference station,

150 particularly in the north-south direction where the geomagnetic field direction changes

151 appreciably with latitude.

152

153 **2.3 DI Correction Using a Least-Squares Method (LS-DI Correction)**

154 Previous studies involving stationary magnetic observations at volcanoes, such as Sasai

155 and Ishikawa (1976), Tanaka et al. (1978), and Davis et al. (1979), estimated correction

156 coefficients using a least-squares approach to account for the DI effect. However, this

157 method has not been applied to regional magnetic surveys. Therefore, we extend the

158 approach to regional total-field magnetic surveys (hereafter referred to as "LS-DI

159 correction"). From Eq. (3), the corrected magnetic anomaly can be written as

$$T_{anm}(t,\mathbf{x}) - T_{dv}(t) = \mathbf{K}\cdot\mathbf{B_{dv}}(t) + C \quad (4)$$

where the unknown parameters $\mathbf{K}$ and C are constant and estimated using the least-squares method:

$$\mathbf{K}, C = \underset{\mathbf{K},C}{\operatorname{argmin}}\left[\sum_t \{T_{anm}(t,\mathbf{x}) - T_{dv}(t) - \mathbf{K}\cdot\mathbf{B_{dv}}(t) - C\}^2\right].$$

Once the optimal coefficients have been determined, the corrected total-field magnetic anomaly can be obtained from Eq. (4) as

$$T_{anm}(t,\mathbf{x}) - T_{dv}(t) - \mathbf{K}\cdot\mathbf{B_{dv}}(t).$$

2.4 DI Correction Using the IGRF (IGRF-DI Correction)

In the LS-DI correction described in section 2.3, the coefficients $\mathbf{K}$ and C are estimated as constant values using least squares. However, for regional surveys, it is necessary to account for the fact that $\mathbf{B_c}(\mathbf{x})$ varies spatially and that $\mathbf{B_m}(t,\mathbf{x})$ varies both spatially and temporally.

To address this issue, we propose an "IGRF-DI correction" method, which assumes that the direction of the main geomagnetic field can be approximated by the International Geomagnetic Reference Field (IGRF) direction at a given location and

time. Specifically, using the IGRF-derived unit direction vector $\widehat{\mathbf{B}}_{\mathbf{IGRF}}(t, \mathbf{x})$ corresponding to each observation location and time, and assuming that

$$\widehat{\mathbf{B}}_{\mathbf{m}}(t, \mathbf{x}) \approx \widehat{\mathbf{B}}_{\mathbf{IGRF}}(t, \mathbf{x}),$$

the diurnal variation term $\widehat{\mathbf{B}}_{\mathbf{IGRF}}(t, \mathbf{x}) \cdot \mathbf{B}_{\mathbf{dv}}(t)$ can be directly calculated by projecting the observatory-derived vector variation onto the local IGRF direction. Substituting this term into Eq. (2), the corrected total-field magnetic anomaly is obtained as

$$T_{anm}(t, \mathbf{x}) - \widehat{\mathbf{B}}_{\mathbf{IGRF}}(t, \mathbf{x}) \cdot \mathbf{B}_{\mathbf{dv}}(t).$$

Because the direction of the main geomagnetic field is strongly influenced by latitudinal variations in magnetic inclination, the proposed method is expected to be particularly effective when survey areas are distributed over a wide north-south extent relative to the reference station.

3 Data Processing

This section describes the data processing workflow, which is summarized in the flowchart shown in Fig. 1. In this study, we used total magnetic intensity data acquired during the GS24 cruise (Sato et al., 2026) and the GB25 cruise (Ono et al., submitted).

191 The survey areas are outlined by blue rectangles in Fig. 2. Total magnetic intensity data
192 were collected using a towed cesium magnetometer. The raw data were first resampled
193 at 1-min intervals and corrected for sensor tow distance. Total-field magnetic anomalies
194 were then calculated by subtracting the International Geomagnetic Reference Field
195 (IGRF14; International Association of Geomagnetism and Aeronomy, 2024), which
196 was used as the reference main field: $\|\mathbf{B_m}(t, \mathbf{x})\| = T_{IGRF}(t, \mathbf{x})$.
197 Next, geomagnetic observatory data from Okinawa, Kanoya, Kakioka, and
198 Memambetsu, arranged from south to north, were used to derive the diurnal variation
199 correction (Geospatial Information Authority of Japan, 2026; Kakioka Magnetic
200 Observatory, 2013 a, b, c). Because these observatories span a wide latitudinal range
201 (Fig. 2), the correction was performed using data from each observatory separately to
202 evaluate the influence of magnetic inclination on the correction results. The diurnal
203 variations recorded at each observatory are shown in Fig. 3 (Geospatial Information
204 Authority of Japan, 2026; Kakioka Magnetic Observatory, 2013a,b,c).
205 As evident from Fig. 3, geomagnetic activity was relatively high during both the GS24
206 and GB25 cruises. In particular, the GS24 survey period included a geomagnetic storm,

207 producing large-amplitude magnetic-field variations and making these datasets well
208 suited for evaluating the performance of diurnal variation correction methods. The
209 diurnal variation at each observatory was calculated by subtracting the annual mean
210 magnetic field value for the corresponding survey year. The annual mean
211 constants, T_{base} and $\mathbf{B_{base}}$ used for each observatory are listed in Table 1.
212 Using the geomagnetic observatory data described above, three diurnal variation
213 correction methods, namely the conventional diurnal variation correction (CDV
214 correction), least-squares DI correction (LS-DI correction), and IGRF-based DI
215 correction (IGRF-DI correction), were applied to the magnetic data from both cruises.
216 To evaluate the performance of each correction method, the root mean square (RMS)
217 crossover error was calculated for the datasets corrected using data from each
218 geomagnetic observatory. Ideally, the RMS crossover error approaches zero as the
219 correction becomes more effective. Crossover errors were extracted using the x2sys
220 program (Wessel, 2010).
221 In addition, the predicted coefficient

$$\mathbf{K_{IGRF}}(t_0, \mathbf{x}_0) = \widehat{\mathbf{B}}_{\mathbf{IGRF}}(t_0, \mathbf{x}_0) - \widehat{\mathbf{B}}_{\mathbf{base}} \quad (5)$$

222 was calculated, where $\widehat{\mathbf{B}}_{\mathbf{IGRF}}(t_0, \mathbf{x}_0)$ is IGRF direction vector at a representative time

223 t_0 and location $\mathbf{x}_0$ within each survey area. The representative $\mathbf{x}_0$ and t_0 are

224 126°30′E, 26°00′N, at sea level (0 m altitude) on 11 November 2025 for the GB25

225 cruise and 129°30′E, 32°30′N, at sea level (0 m altitude) on 6 October 2024 for the

226 GS24 cruise, respectively (Fig. 2). The resulting predicted coefficients, $\mathbf{K}_{\mathbf{IGRF}}(t_0, \mathbf{x}_0)$

227 are listed in Table 1. These predicted values were then compared with the estimated

228 coefficients, $\mathbf{K}$.

229 To further quantify the difference in geomagnetic field direction between the survey

230 area and each reference observatory, the angular

231 difference $\Delta\theta$ between $\widehat{\mathbf{B}}_{\mathbf{IGRF}}(t_0, \mathbf{x}_0)$ and $\widehat{\mathbf{B}}_{\mathbf{base}}$ was calculated as

232 $$\Delta\theta(t_0, \mathbf{x}_0) = \cos^{-1}\left(\widehat{\mathbf{B}}_{\mathbf{IGRF}}(t_0, \mathbf{x}_0) \cdot \widehat{\mathbf{B}}_{\mathbf{base}}\right).$$

233 Because of eq. (5), the angular difference can alternatively be expressed as

$$\Delta\theta(t_0, \mathbf{x}_0) = 2\sin^{-1}\left(\frac{\|\mathbf{K}_{\mathbf{IGRF}}(t_0, \mathbf{x}_0)\|}{2}\right). \quad (6)$$

234 The resulting values of $\Delta\theta(t_0, \mathbf{x}_0)$ are listed in Table 1 and compared with the

235 reduction in crossover RMS achieved by the IGRF-DI correction relative to the

236 conventional CDV correction.

4 Results

4.1 GS24 Cruise

The results for the GS24 cruise are shown in Figs. 4 and 5. Because magnetic observations were conducted continuously throughout the day during the GS24 cruise, the amplitude of the diurnal variation was large, resulting in a high pre-correction crossover RMS of 58.74 nT. In addition, stripe-like artifacts elongated along the survey lines are visible in many parts of the anomaly map. Among the corrected results shown in Fig. 5(b)–(m), the KNY IGRF-DI correction (Fig. 5j) yielded the lowest crossover RMS of 7.36 nT. Compared with the uncorrected data, the magnetic anomaly contours became noticeably smoother after correction.

Figure 6 shows histograms of crossover differences before and after correction. The KNY IGRF-DI result (Fig. 6j) exhibits the narrowest distribution and the smallest crossover errors, confirming its superior correction performance.

When the three correction methods are compared for each observatory, the correction performance generally improves as the reference observatory becomes closer to the

253 survey area, following the order MMB, KAK, OKI, and KNY (Fig. 6). Furthermore, the
254 IGRF-DI correction consistently outperforms the conventional diurnal variation
255 correction (CDV correction) for all four observatories. In contrast, the performance of
256 the LS-DI correction varies substantially among observatories. For the distant MMB
257 and KAK observatories, the LS-DI correction produced the lowest crossover RMS
258 among the three methods (Figs. 5c,f and 6c,f). However, for the nearby KNY
259 observatory, the LS-DI correction yielded the largest crossover RMS, corresponding to
260 the poorest performance (Figs 5i and 6i). For the OKI observatory, the LS-DI and
261 IGRF-DI corrections resulted in nearly identical crossover RMS values (Figs. 5i,m and
262 6i,m).
263 Comparison of the coefficients estimated by the least-squares DI correction, $\mathbf{K}$, with the
264 values predicted from the representative IGRF field direction of the survey
265 area, $\mathbf{K_{IGRF}}(t_0, \mathbf{x}_0)$, reveals substantial discrepancies. In all cases, $\mathbf{K}$ are considerably
266 larger than $\mathbf{K_{IGRF}}(t_0, \mathbf{x}_0)$ (Table 1). Moreover, the standard deviation of the residuals
267 used in the estimation of $\mathbf{K}$ is approximately 122 nT, indicating a large degree of
268 unexplained variability (Table 1).

269

270 **4.2 GB25 Cruise**

271 The survey tracks and correction results for the GB25 cruise are shown in Figs. 7 and 8.

272 During the GB25 cruise, magnetic observations were conducted primarily at night,

273 resulting in a relatively small crossover RMS of 22.52 nT before diurnal variation

274 correction (Figs. 8a and 9a). Nevertheless, the magnetic anomaly map contains

275 numerous areas where the contours appear irregular and discontinuous (Fig. 8a).

276 Among the corrected results shown in Fig. 8(b)–(m), the OKI IGRF-DI correction

277 yielded the lowest crossover RMS of 4.81 nT (Figs. 8m and 9m) and the anomaly

278 contours became noticeably smoother compared with the uncorrected data.

279 For almost all correction methods, the correction performance generally improves as the

280 reference observatory becomes closer to the survey area, following the order MMB,

281 KAK, KNY, and OKI. The only exception is the LS-DI correction, for which the KNY

282 result is slightly better than the OKI result (Figs. 8i,l and 9i,l). Comparisons between the

283 CDV and IGRF-DI corrections, as well as between the LS-DI and IGRF-DI corrections,

284 show that the IGRF-DI correction consistently yields lower crossover RMS values in all

285 cases. In particular, for the nearby KNY and OKI observatories, the LS-DI correction

286 produces the largest crossover RMS among the three methods, indicating the poorest

287 correction performance.

288 Comparison of the coefficients estimated by LS-DI correction, $\mathbf{K}$, with the coefficients

289 predicted from the representative IGRF field direction of the survey

290 area, $\mathbf{K_{IGRF}}(t_0, \mathbf{x}_0)$, reveals substantial discrepancies as well as GS24 cruise. The

291 estimated $\mathbf{K}$ values are consistently much larger than the corresponding

292 $\mathbf{K_{IGRF}}(t_0, \mathbf{x}_0)$. In particular, coefficients for the MMB observatory exceed the

293 theoretical upper bound:

294 $$\|\mathbf{K}\| \leq 2$$

295 derived from Eq. (6), suggesting that the least-squares estimation is influenced by

296 factors other than the DI effect. Furthermore, the MMB LS-DI result (Fig. 8d) contains

297 a substantially larger positive anomaly region than the other corrected datasets,

298 suggesting that the recovered anomaly amplitudes may not be physically and

299 theoretically realistic despite the reduced crossover RMS.

In addition, the standard deviation of the residuals used in the coefficient estimation is approximately 52 nT, indicating considerable unexplained variability in the least-squares fitting process (Table 1).

5 Discussion

5.1 Limitations of LS-DI Correction in Regional Total-Field Magnetic Surveys

In the LS-DI correction described in section 2.3, a single coefficient is estimated using all magnetic data acquired during a cruise. However, because crustal magnetic anomalies vary spatially, the coefficient $\mathbf{K}$ should, in principle, be estimated for each location. To address this issue, we also investigated a moving-window approach in which $\mathbf{K}$ is estimated independently within each window. Furthermore, to improve the stability and convergence of the estimation, a weighting constraint based on the coefficient predicted from the IGRF was introduced. The formulation is given below:

$$\mathbf{K}(t,\mathbf{x}_t), C(t,\mathbf{x}_t) = \underset{\mathbf{K},C}{\operatorname{argmin}} \left[\sum_{i=t-L}^{t+L} \{T_{anm}(i,\mathbf{x}_i) - T_{dv}(i) - \mathbf{K}\cdot\mathbf{B_{dv}}(i) - C\}^2 + \lambda \|\mathbf{K} - \mathbf{K_{IGRF}}(t,\mathbf{x}_t)\|^2 \right],$$

where L is the half-window lengths, λ is the weighting parameter, and $\mathbf{x}_i$ and $\mathbf{x}_t$ are locations at time i and t, respectively. This formulation becomes equivalent to the

316 original LS-DI correction when $\lambda = 0$ and the window length $2L$ spans the entire
317 observation period. The coefficient estimation was performed using this moving-
318 window approach in which the analysis window was shifted at 1-min intervals along the
319 time series.
320 Figure 10 shows an example of the moving-window LS-DI correction applied to the
321 GS24 cruise using data from the MMB observatory, for which the original LS-DI
322 correction substantially reduced the crossover RMS. In all three tested configurations,
323 the estimated coefficient $\mathbf{K}$ exhibits pronounced spatial variations that closely
324 correspond to variations in the crustal magnetic field (Fig. 10b,c,d,g). This result
325 suggests that the temporal variation associated with diurnal magnetic fields and the
326 apparent temporal variation caused by spatial changes in crustal magnetic anomalies
327 along the survey track are not sufficiently separated during the coefficient estimation
328 process. Consequently, the estimated $\mathbf{K}$ values are influenced by crustal magnetic
329 anomalies as well as external-field variations. As a result, the residual standard
330 deviation increases in regions where the crustal magnetic field exhibits large spatial
331 variations (Fig. 10f). Although the moving-window approach and IGRF-based

regularization improve the locality and stability of the estimation, they do not fully eliminate this ambiguity, indicating an inherent difficulty in obtaining physically meaningful coefficients solely through least-squares estimation in regional moving-platform surveys.

5.2 Which Method Is Most Appropriate for Diurnal Variation Correction?

In this section, we discuss which diurnal variation correction method is most appropriate for regional total-field magnetic surveys. Section 5.1 demonstrated a fundamental limitation of applying LS-DI correction to regional surveys, namely that least-squares estimation cannot reliably separate external-field variations from spatial variations in crustal magnetic anomalies. Therefore, the following discussion focuses on a comparison between the CDV correction and the IGRF-DI correction.

Figure 11 shows the relationship between the representative angular difference, $\Delta\theta(t_0, \mathbf{x}_0)$, and the difference in crossover RMS between the CDV and IGRF-DI corrections. In all cases examined in this study, the IGRF-DI correction yielded lower crossover RMS values than the conventional CDV correction. Furthermore, for both

348 cruises, the difference in correction performance generally increased with increasing
349 $\Delta\theta(t_0, \mathbf{x}_0)$. These results indicate that correction of the DI effect is important not only
350 for stationary magnetic observations but also for regional moving-platform magnetic
351 surveys.
352 In this study, we assume that the external-field variation vector, $\mathbf{B_{dv}}(t)$, is identical at
353 the reference observatory and the survey location. However, Fig. 3 shows that the
354 amplitudes and timings of the component variations differ substantially among
355 observatories. These spatial differences in $\mathbf{B_{dv}}(t)$ are one of the factors responsible for
356 the increase in crossover RMS when more distant observatories are used as reference
357 stations in both cruises. Ideally, the reference observatory should be located at the
358 survey area itself. In marine magnetic surveys, however, establishing a nearby reference
359 station is usually impractical, and therefore data from land-based geomagnetic
360 observatories are commonly used. Under such circumstances, the use of data from the
361 nearest available geomagnetic observatory is expected to provide the most reliable
362 correction as previous studies have suggested (e.g., Sergipe et al., 2021).

363 Based on these results, we recommend that diurnal variation correction for regional
364 total-field magnetic surveys should, in general, be performed using the IGRF-DI
365 correction together with vector magnetic-field data from the nearest available
366 geomagnetic observatory. Because the method requires no empirical coefficient
367 estimation and can be implemented directly from observatory and IGRF data, it
368 provides a practical and physically based approach to diurnal variation correction. This
369 approach can therefore be regarded as the default strategy for regional magnetic
370 surveys.
371
372 **5.3 Implications for General Regional Total-Field Magnetic Surveys**
373 In this study, we focused on DI correction for regional marine magnetic surveys.
374 However, deep-sea total-field magnetic surveys conducted using manned submersibles
375 and autonomous underwater vehicles (AUVs), as well as regional airborne magnetic
376 surveys, employ fundamentally the same principles for diurnal variation correction as
377 marine magnetic surveys. In these applications, corrections are also commonly based on
378 total-field magnetic variations recorded at geomagnetic observatories. To our

knowledge, DI correction methods have not previously been applied to these types of surveys. Although no case study is presented here, the IGRF-DI correction is expected to provide similar benefits when the reference observatory is located far from the observation area. The method proposed in this study therefore has the potential to improve the accuracy of diurnal variation correction for general regional total-field magnetic surveys.

6 Conclusion

We systematically compared three methods for correcting diurnal variations in regional moving-platform total-field magnetic surveys: conventional diurnal variation correction (CDV correction), least-squares DI correction (LS-DI correction), and IGRF-based DI correction (IGRF-DI correction). The three methods were applied to two marine magnetic surveys using vector magnetic-field data from four geomagnetic observatories distributed over a wide latitudinal range, and their performance was evaluated primarily on the basis of crossover RMS differences.

394 The comparison showed that the IGRF-DI correction consistently produced lower
395 crossover RMS values than the CDV correction for both surveys and all four reference
396 observatories. The improvement generally increased with the angular difference in
397 main-field direction between the survey area and reference observatory. These results
398 demonstrate that differences in geomagnetic-field direction can leave appreciable
399 residual external-field variations after conventional correction and that the DI effect
400 should be considered in regional moving-platform total-field magnetic surveys.
401 The performance of the LS-DI correction varied substantially among reference
402 observatories. Although the method occasionally produced considerable reductions in
403 crossover RMS, the estimated coefficients differed markedly from the corresponding
404 values predicted from the IGRF. Moving-window analyses further showed that the
405 least-squares coefficients were influenced by spatial variations in crustal magnetic
406 anomalies. Therefore, a reduction in crossover RMS alone does not necessarily indicate
407 a physically valid correction, because least-squares regression may remove part of the
408 crustal magnetic signal together with the external-field variation. These findings

indicate a fundamental limitation of empirically estimating DI correction coefficients from regional moving-platform survey data.

Among the three methods examined, the IGRF-DI correction provides the most physically based and robust approach because it accounts for the local geomagnetic-field direction at each survey location and observation time without estimating empirical coefficients from the survey data. Spatial differences in external-field variations between the reference observatory and survey area nevertheless remain a source of uncertainty that cannot be eliminated solely by correcting for differences in main-field direction. We therefore recommend applying the IGRF-DI correction using vector magnetic-field data from the nearest suitable geomagnetic observatory as a practical default strategy for regional total-field magnetic surveys. Although further validation is required for airborne and deep-sea applications, the formulation is transferable in principle to a broad range of moving-platform total-field magnetic surveys.

Acknowledgements

We thank the captains, crews, technicians, scientists, and students on board during the GS24 and GB25 cruises.

Author contributions

SO proposed the idea and drafted the initial paper. SO, TS, and HK collected magnetic data. SO, TS, HK, SA, and SN contributed to the interpretation of the results and reviewed the manuscript. All authors approved the published version of the manuscript.

Funding

This work was supported by the GSJ (AIST) geological mapping program.

Availability of data and materials

The datasets used in this study are available from the corresponding author on reasonable request.

Declarations

Competing interests

All authors declare no competing interest.

References

Davis, P.M., Stacey, F.D., Zablocki, C.J., Olson, J.V., (1979). Improved signal discrimination in tectonomagnetism: discovery of a volcanomagnetic effect at Kilauea, Hawaii. Phys. Earth Planet. Inter. 19:331–336. https://doi.org/10.1016/0031-9201(79)90005-0.

GEBCO Compilation Group (2025), GEBCO 2025 Grid. https://download.gebco.net (Accessed: 2026-03-16)

Geospatial Information Authority of Japan (2026), Geomagnetic continuous observation data (raw data) [dataset], Geospatial Information Authority of Japan, doi:10.57499/GSI_GMAG_2026_001.

International Association of Geomagnetism and Aeronomy (2024), IGRF-14. Zenodo. https://doi.org/10.5281/zenodo.14012302

Kakioka Magnetic Observatory (2013a), Kanoya geomagnetic field 1-minute digital data in IAGA-2002 format [dataset], Kakioka Magnetic Observatory Digital Data Service, doi:10.48682/186fd.3f000

Kakioka Magnetic Observatory (2013b), Kakioka geomagnetic field 1-minute digital data in IAGA-2002 format [dataset], Kakioka Magnetic Observatory Digital Data Service, doi:10.48682/186bd.3f000

Kakioka Magnetic Observatory (2013c), Memambetsu geomagnetic field 1-minute digital data in IAGA-2002 format [dataset], Kakioka Magnetic Observatory Digital Data Service, doi:10.48682/186d7.3f000

Sasai, Y and Ishikawa, Y (1976), Repeated Magnetic Survey of the Total Force Intensity in the Boso Peninsula: 1968-1976.

Sato, T and Koge, H (2026) Preliminary results of a magnetic anomaly survey off Northwest Kyushu during cruises GS24 and GB24. Bulletin of the Geological Survey of Japan, vol. 77 (3/4), p. xx–xx, 2026

Sergipe, P. P., Marangoni, Y. R., Dos Santos, R. P. Z., De Moura, D. S., & Jovane, L. (2021). Diurnal variation effect in marine magnetometric surveys: clues from surveys in southeast Brazil. Marine Geophysical Research, 42(3), 28.

Takahashi K, Takakura S, Matsushima N, Fujii I (2018) Relationship between volcanic activity and shallow hydrothermal system at Meakandake volcano, Japan, inferred from geomagnetic and audio-frequency magnetotelluric measurements. Journal of Volcanology and Geothermal Research 349:351–369. https://doi.org/10.1016/j.jvolgeores.2017.11.019

Tanaka, Y., Masuda, H., Kawamura, M., Ohchi, K., Kato, S., Baba, H., (1978). Surveys of geomagnetic total intensity with proton precession magnetometers on Aso volcano. Report of 1st Joint Geophysical and Geochemical Observations of Aso Volcano, pp. 31–39 (in Japanese).

Wessel, P. (2010) Tools for analyzing intersecting tracks: The x2sys package. *Computers and Geosciences*, **36**(3), 348–354.

Wessel, P., Luis, J. F., Uieda, L., Scharroo, R., Wobbe, F., Smith, W. H. F., and Tian, D (2019) The Generic Mapping Tools version 6. *Geochemistry, Geophysics, Geosystems*, **20**, 5556–5564.

Fig. 1. Overview of workflow for diurnal variation correction. Abbreviations are explained in the Method and Data processing sections.

Fig. 2. Location map of the survey areas and observatory stations. Blue rectangles show the survey area during the GS24 and GB25 cruise. Red stars indicate the reference observation stations: Okinawa (OKI), Kanoya (KNY), Kakioka (KAK), and Memambetsu (MMB). Red circles indicate the representative points of each cruise. Gray areas represent regions above sea level.

Fig. 3. Diurnal variations during the GS24 (left) and GB25 (right) cruises at Okinawa (red lines), Kanoya (orange lines), Kakioka (green lines), and Memambetsu (blue lines)

500 observatories. From top to bottom, the panels show the diurnal variations of the X

501 (North), Y (East), Z (Down) components and the total magnetic intensity [(nT]). The

502 constant values (T_{base} and $\mathbf{B_{base}}$) were subtracted to derive the diurnal variations for

503 each cruise and observatory; these values are listed in Table 1.

504

505 Fig. 4. Comparison of magnetic anomaly data before and after diurnal variation and DI

506 corrections during the GS24 cruise from 06:00 UTC on 10 October to 06:00 UTC on 11

507 October 2024. From top to bottom, the panels show results obtained using data from the

508 (a) Memambetsu (MMB), (b) Kakioka (KAK), (c) Kanoya (KNY), and (d) Okinawa

509 (OKI) geomagnetic observatories, respectively. Black curves show the data before

510 diurnal variation correction, green curves show the data after CDV-correction, red

511 curves show the results after the LS-DI correction, and blue curves show the results

512 after IGRF-DI correction.

513

514 Fig. 5. Total magnetic anomaly maps and ship track lines during the GS24 cruise. Color

515 palette for bathymetry is same to Fig.1. (a) Total magnetic anomaly before diurnal

516 variation correction. Panels (b)–(d) show the total magnetic anomaly after (b) CDV, (c)
517 LS-DI, and (d) IGRF-DI correction using Memambetsu (MMB) observatory data.
518 Panels (e)–(g) show the total magnetic anomaly after (e) CDV, (f) LS-DI, and (g)
519 IGRF-DI correction using Kakioka (KAK) observatory data. Panels (h)–(j) show the
520 total magnetic anomaly after (h) CDV, (i) LS-DI, and (j) IGRF-DI correction using
521 Kanoya (KNY) observatory data. Panels (k)–(m) show the total magnetic anomaly after
522 (k) CDV, (l) LS-DI, and (m) IGRF-DI correction using Okinawa (OKI) observatory
523 data. Panels (a')–(m') show the enlarged shaded map of panels (a)–(m), respectively.
524 Enlarged area is shown as red rectangle in ship track map. Illumination is from the
525 North-East.
526
527 Fig. 6. Histograms of cross-over differences (CODs) during the GS24 cruise. (a)
528 Histograms of CODs before correction. (b–d) Histograms of CODs after (b) CDV, (c)
529 LS-DI, and (d) IGRF-DI correction using data of MMB stations, respectively. (e–g)
530 Histograms of CODs after (e) CDV, (f) LS-DI, and (g) IGRF-DI correction using data
531 of KAK stations, respectively. (h–j) Histograms of CODs after (h) CDV, (i) LS-DI, and

(j) IGRF-DI correction using data of KNY stations, respectively. (k–m) Histograms of CODs after (k) CDV, (l) LS-DI, and (m) IGRF-DI correction using data of OKI stations, respectively. The RMS of CODs is indicated in each panel.

Fig. 7. Comparison of magnetic anomaly data before and after CDV, LS-DI, and IGRF-DI corrections during the GB25 cruise from 12:00 UTC on 4 November to 12:00 UTC on 5 November 2025. The other details are the same as in Fig. 4.

Fig. 8. Total magnetic anomaly maps and ship track lines during the GB25 cruise. The other details are the same as in Fig. 5.

Fig. 9. Histograms of cross-over differences (CODs) during the GB25 cruise. The other details are the same as in Fig. 6.

Fig. 10. Example of moving-window LS-DI correction with different regularization parameters λ and half-window lengths L [min]. For data sampled at 1-min intervals, a

548 half-window length of L corresponds to a maximum window size of $2L + 1$ data

549 points. The results were obtained by applying the correction to data from the

550 Memambetsu (MMB) observatory during the GS24 cruise. (a) Observed variations in

551 the three magnetic-field components (X_{dv}, Y_{dv}, Z_{dv}) and total magnetic intensity (T_{dv}).

552 (b–d) Estimated coefficients K_x, K_y, and K_z, respectively. The black dashed lines

553 indicate the corresponding reference values derived from the IGRF. Blue, red, and green

554 curves in Fig (b-g) indicate $(\lambda, L) = (10^5, 10)$, $(10^6, 30)$, and $(10^6, 10)$, respectively.

555 (e) Estimated intercept C. (f) Standard deviation of the regression residuals within each

556 sliding window. (g) Magnetic anomalies after CDV correction, after DI correction using

557 only the IGRF-derived coefficients, and after DI correction using the locally estimated

558 coefficients.

559

560 Fig. 11. Relationship between angular difference and RMS difference between CDV

561 correction and IGRF-DI correction. Orange and blue symbols represent the GS24 and

562 GB25 cruises, respectively. Circles, squares, triangles, and diamonds represent data

563 corrected using observatory data from Okinawa (OKI), Kanoya (KNY), Kakioka
564 (KAK), and Memambetsu (MMB), respectively.
565
566 Table 1. Summary of base magnetic field values and parameters for the GS24 and GB25
567 cruises using reference data from the Okinawa (OKI), Kanoya (KNY), Kakioka (KAK),
568 and Memambetsu (MMB) observatories. The definitions of each parameter are
569 described in the Methods and Data Processing Sections. Vector components are listed in
570 the order X (North), Y (East), and Z (Down) from top to bottom.
571
572
573
574
575

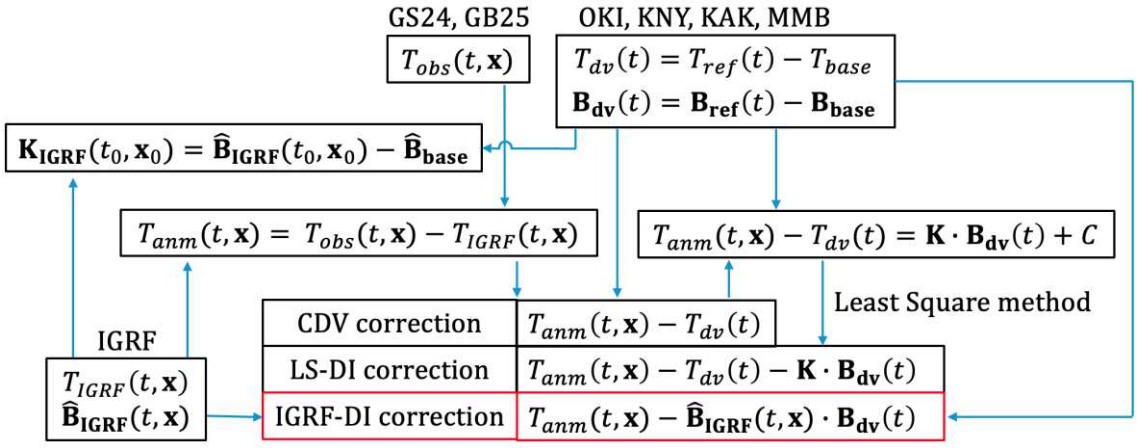
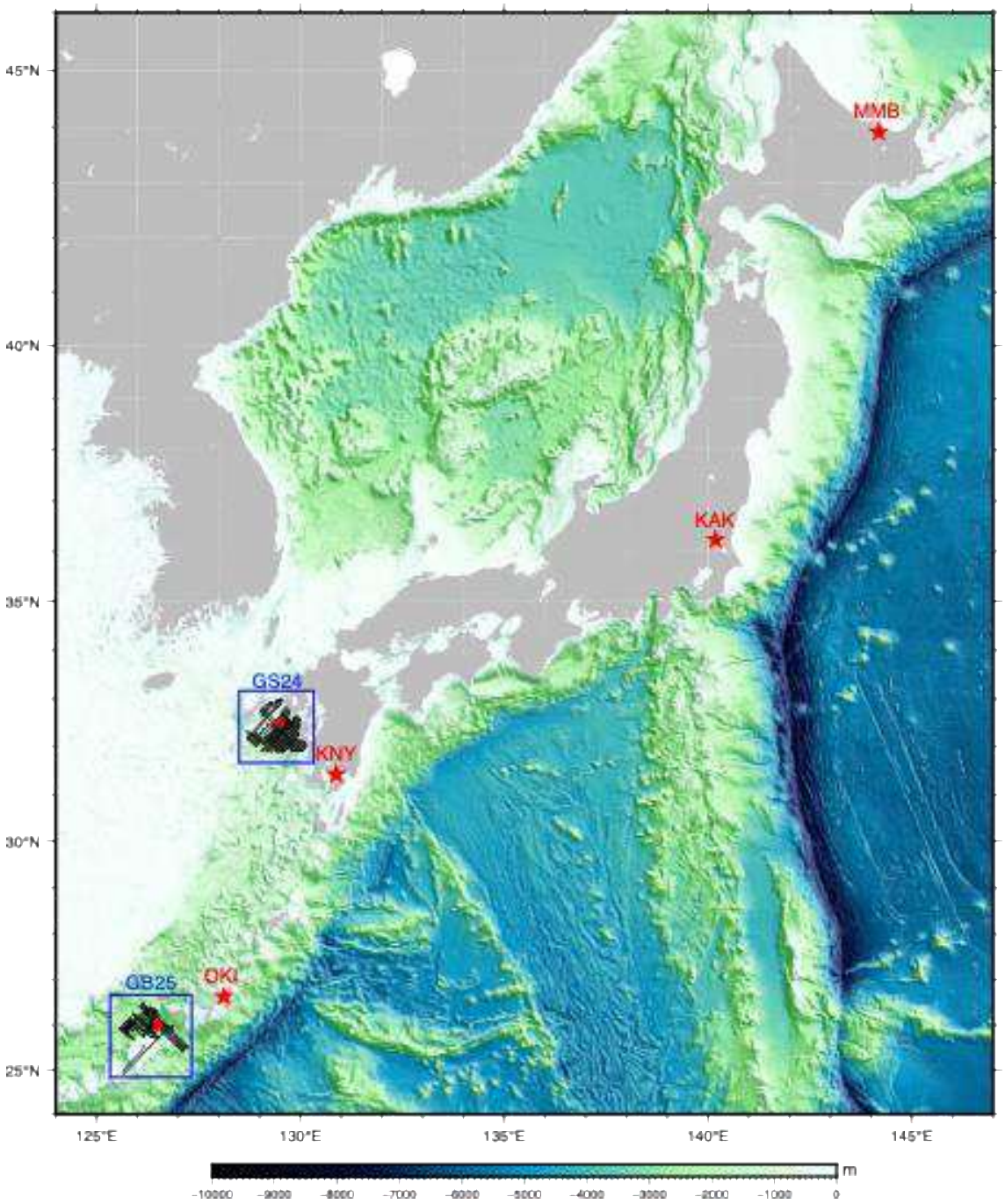


Fig. 1. Overview of workflow for diurnal variation correction. Abbreviations are explained in the Method and Data processing sections.



580

581 Fig. 2. Location map of the survey areas and observatory stations. Blue rectangles show the survey area

582 during the GS24 and GB25 cruise. Red stars indicate the reference observation stations: Okinawa (OKI),

Kanoya (KNY), Kakioka (KAK), and Memambetsu (MMB). Red circles indicate the representative points of each cruise. Gray areas represent regions above sea level.

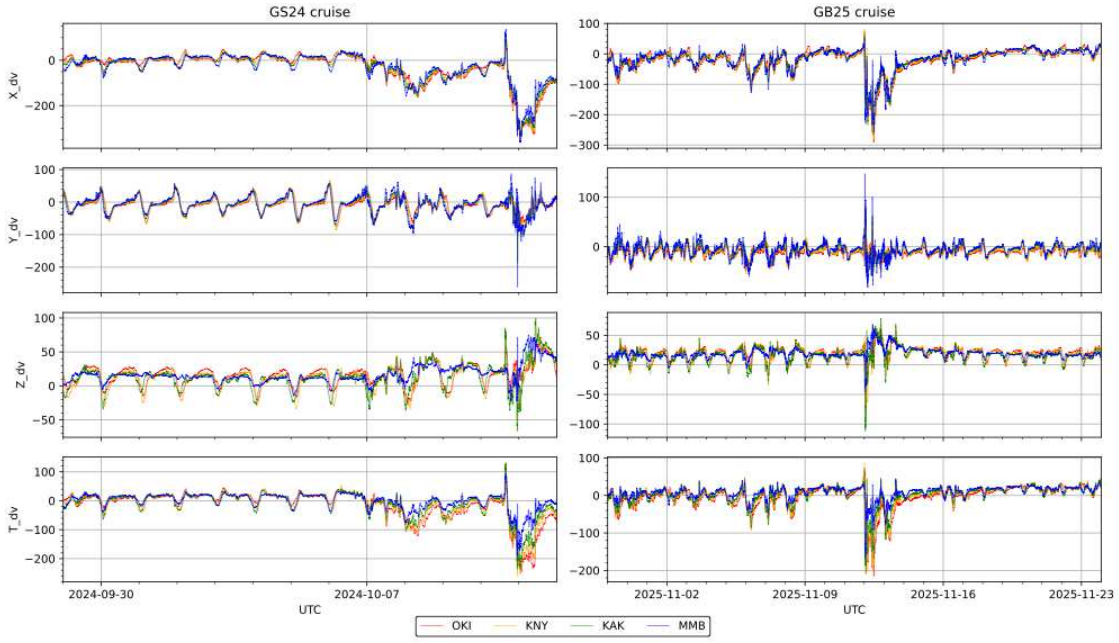
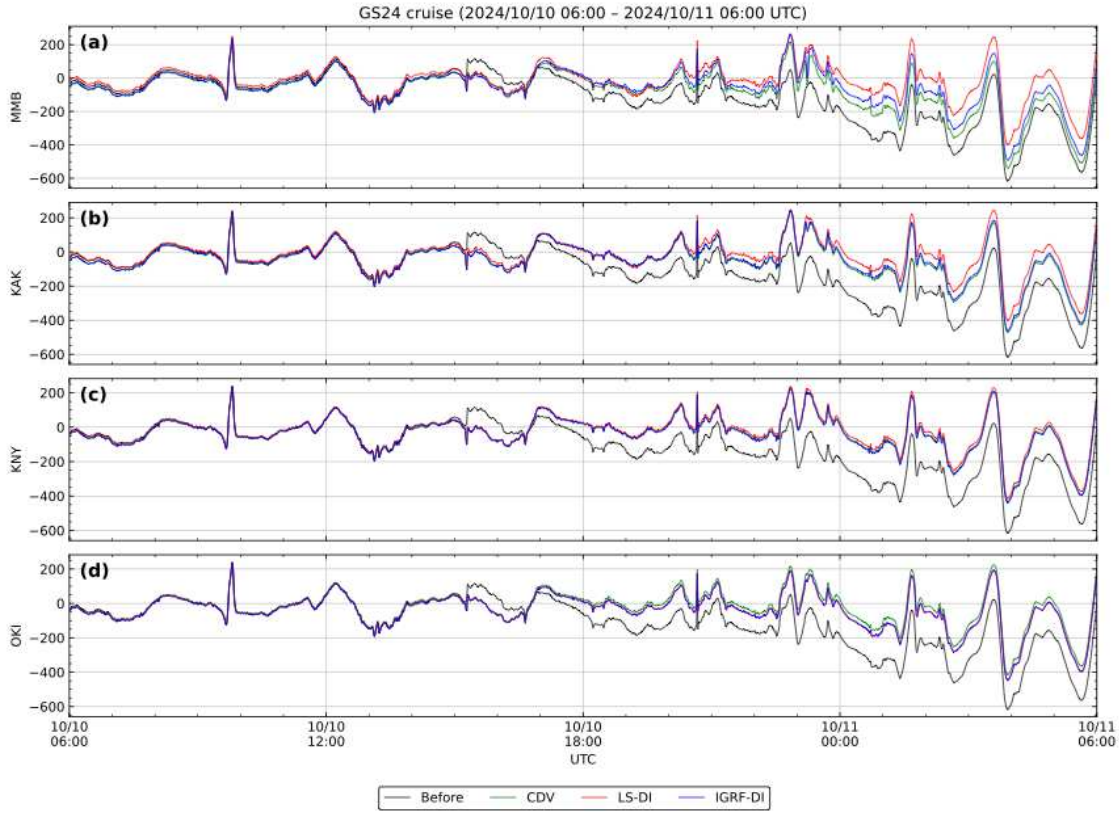


Fig. 3. Diurnal variations during the GS24 (left) and GB25 (right) cruises at Okinawa (red lines), Kanoya (orange lines), Kakioka (green lines), and Memambetsu (blue lines) observatories. From top to bottom, the panels show the diurnal variations of the X (North), Y (East), Z (Down) components and the total magnetic intensity [nT]. The constant values (T_{base} and $\boldsymbol{B_{base}}$) were subtracted to derive the diurnal variations for each cruise and observatory; these values are listed in Table 1.



593

594 Fig. 4. Comparison of magnetic anomaly data before and after diurnal variation and DI corrections during

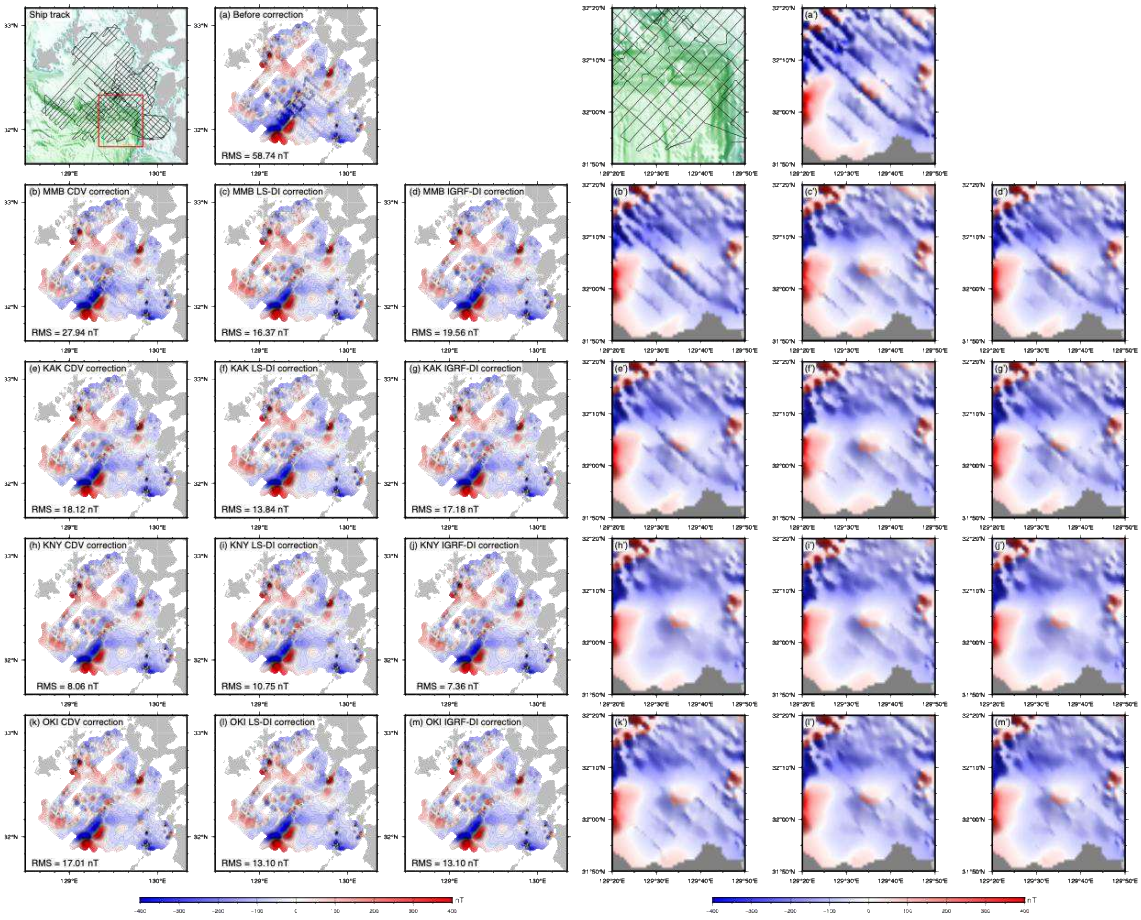
595 the GS24 cruise from 06:00 UTC on 10 October to 06:00 UTC on 11 October 2024. From top to bottom,

596 the panels show results obtained using data from the (a) Memambetsu (MMB), (b) Kakioka (KAK), (c)

597 Kanoya (KNY), and (d) Okinawa (OKI) geomagnetic observatories, respectively. Black curves show the

598 data before diurnal variation correction, green curves show the data after CDV-correction, red curves

599 show the results after the LS-DI correction, and blue curves show the results after IGRF-DI correction.



600

601 Fig. 5. Total magnetic anomaly maps and ship track lines during the GS24 cruise. Color palette for

602 bathymetry is same to Fig.1. (a) Total magnetic anomaly before diurnal variation correction. Panels (b)–

603 (d) show the total magnetic anomaly after (b) CDV, (c) LS-DI, and (d) IGRF-DI correction using

604 Memambetsu (MMB) observatory data. Panels (e)–(g) show the total magnetic anomaly after (e) CDV,

605 (f) LS-DI, and (g) IGRF-DI correction using Kakioka (KAK) observatory data. Panels (h)–(j) show the

606 total magnetic anomaly after (h) CDV, (i) LS-DI, and (j) IGRF-DI correction using Kanoya (KNY)

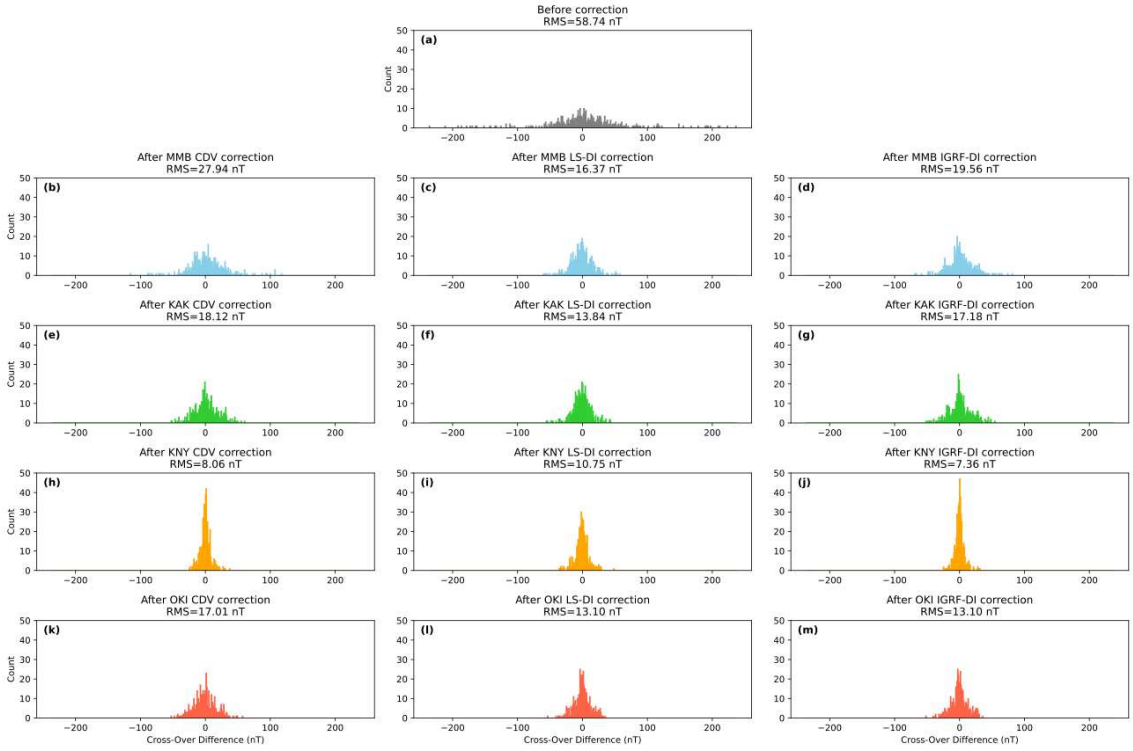
607 observatory data. Panels (k)–(m) show the total magnetic anomaly after (k) CDV, (l) LS-DI, and (m)

608 IGRF-DI correction using Okinawa (OKI) observatory data. Panels (a')–(m') show the enlarged shaded

609 map of panels (a)–(m), respectively. Enlarged area is shown as red rectangle in ship track map.

610 Illumination is from the North-East.

611



612

613 Fig. 6. Histograms of cross-over differences (CODs) during the GS24 cruise. (a) Histograms of CODs

614 before correction. (b–d) Histograms of CODs after (b) CDV, (c) LS-DI, and (d) IGRF-DI correction using

615 data of MMB stations, respectively. (e–g) Histograms of CODs after (e) CDV, (f) LS-DI, and (g) IGRF-

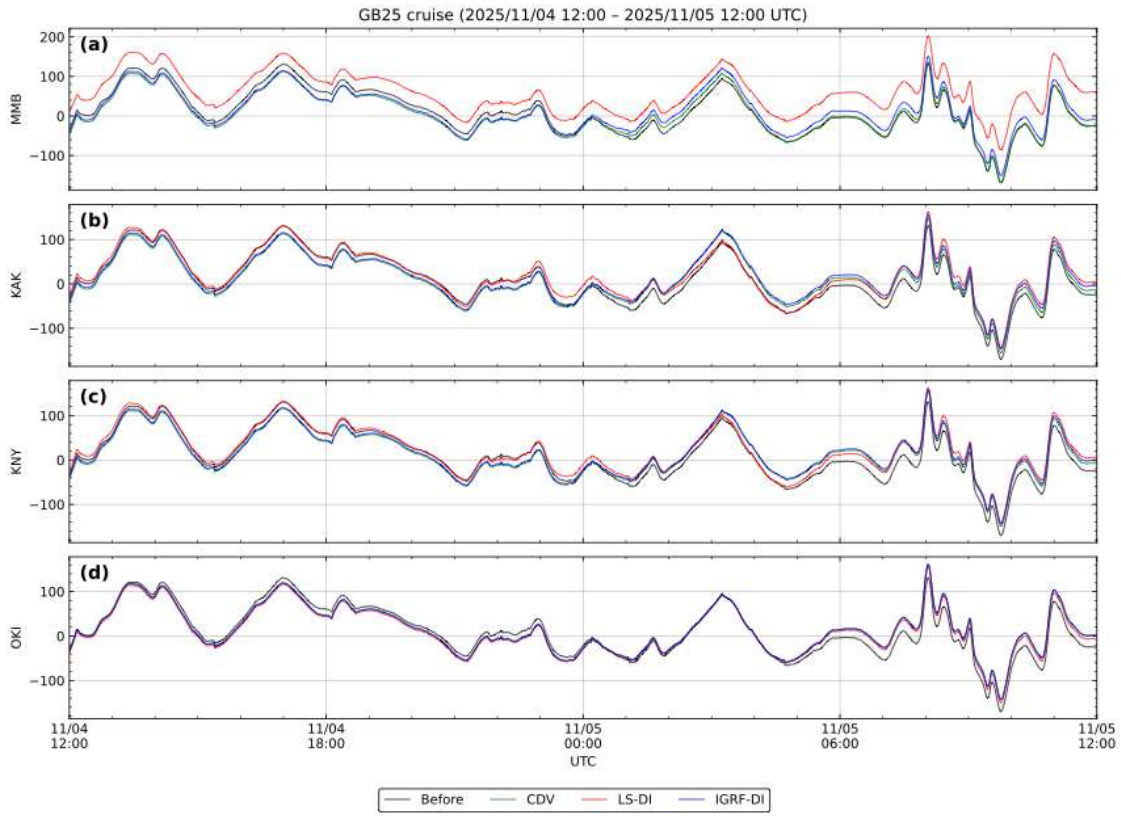
616 DI correction using data of KAK stations, respectively. (h–j) Histograms of CODs after (h) CDV, (i) LS-

617 DI, and (j) IGRF-DI correction using data of KNY stations, respectively. (k–m) Histograms of CODs

618 after (k) CDV, (l) LS-DI, and (m) IGRF-DI correction using data of OKI stations, respectively. The RMS

619 of CODs is indicated in each panel.

620



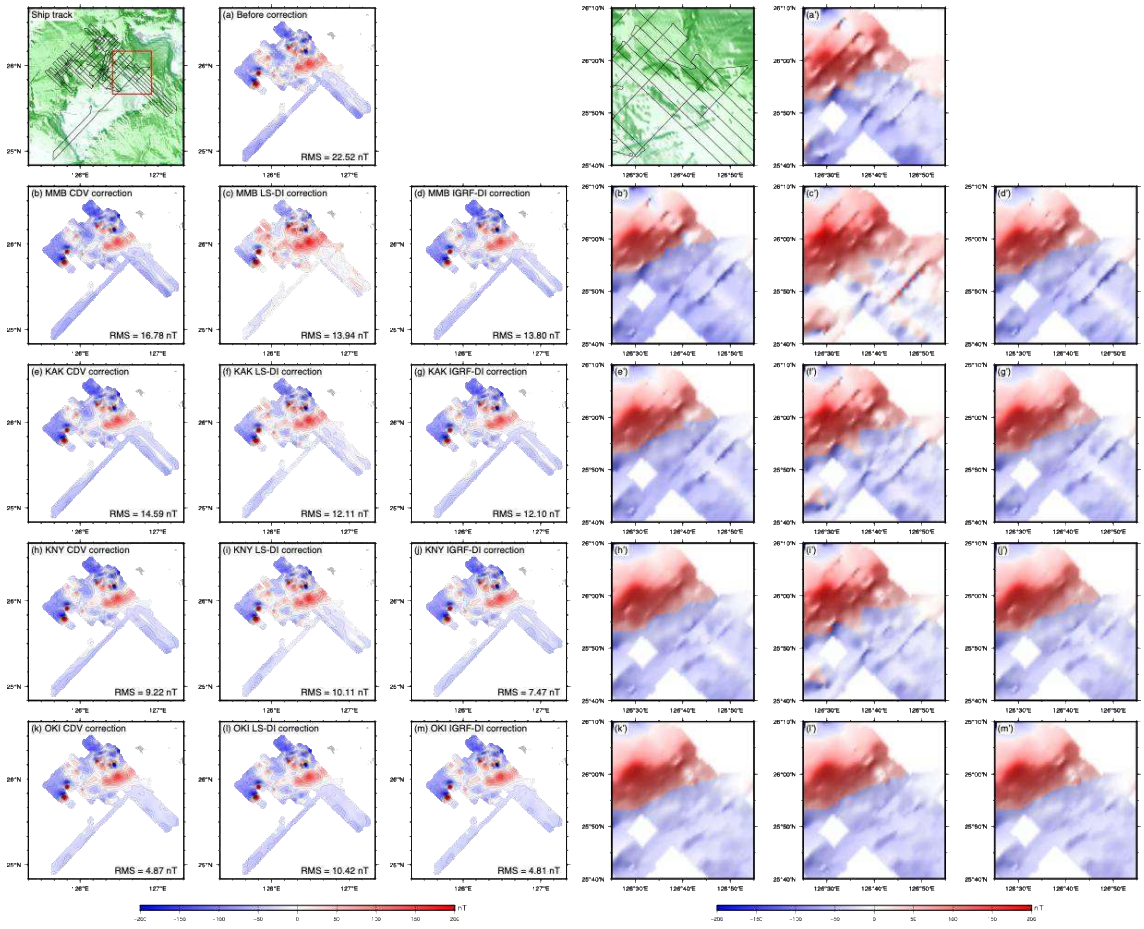
621

622 Fig. 7. Comparison of magnetic anomaly data before and after CDV, LS-DI, and IGRF-DI corrections

623 during the GB25 cruise from 12:00 UTC on 4 November to 12:00 UTC on 5 November 2025. The other

624 details are the same as in Fig. 4.

625

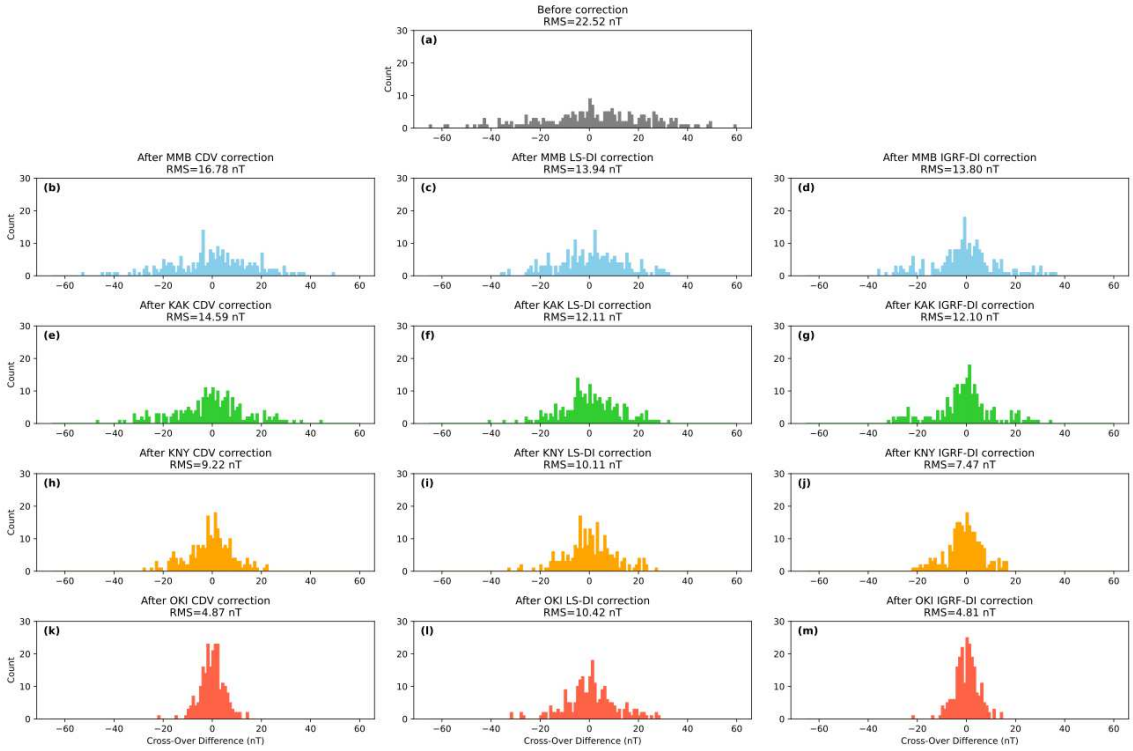


626

627 Fig. 8. Total magnetic anomaly maps and ship track lines during the GB25 cruise. The other details are

628 the same as in Fig. 5.

629



630

631 Fig. 9. Histograms of cross-over differences (CODs) during the GB25 cruise. The other details are the

632 same as in Fig. 6.

633

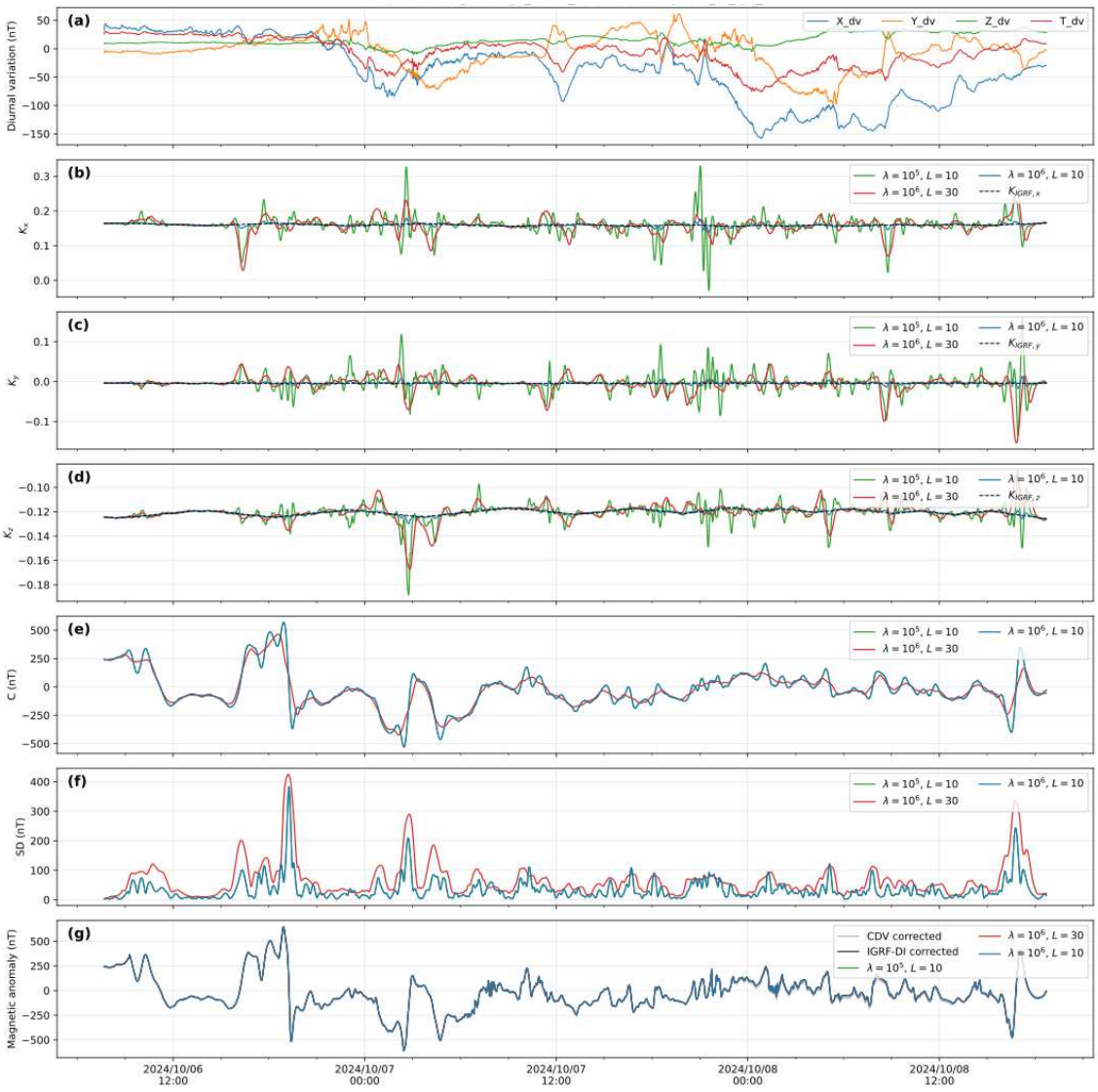


Fig. 10. Example of moving-window LS-DI correction with different regularization parameters λ and half-window lengths L [min]. For data sampled at 1-min intervals, a half-window length of L corresponds to a maximum window size of $2L + 1$ data points. The results were obtained by applying the correction to data from the Memambetsu (MMB) observatory during the GS24 cruise. (a) Observed variations in the three magnetic-field components (X_{dv}, Y_{dv}, Z_{dv}) and total magnetic intensity (T_{dv}). (b–d) Estimated coefficients K_x, K_y, and K_z, respectively. The black dashed lines indicate the corresponding

reference values derived from the IGRF. Blue, red, and green curves in Fig (b-g) indicate $(\lambda, L) =$ $(10^5, 10)$, $(10^6, 30)$, and $(10^6, 10)$, respectively. (e) Estimated intercept C. (f) Standard deviation of the regression residuals within each sliding window. (g) Magnetic anomalies after CDV correction, after DI correction using only the IGRF-derived coefficients, and after DI correction using the locally estimated coefficients.

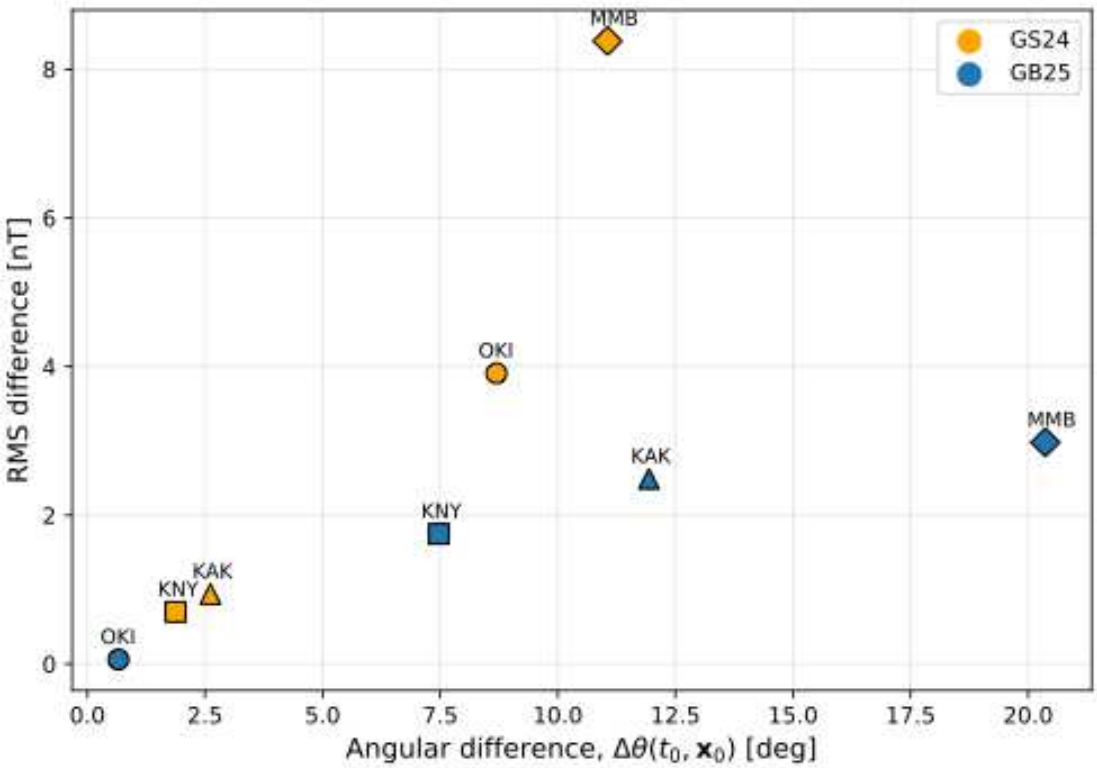


Fig. 11. Relationship between angular difference and RMS difference between CDV correction and IGRF-DI correction. Orange and blue symbols represent the GS24 and GB25 cruises, respectively.

Circles, squares, triangles, and diamonds represent data corrected using observatory data from Okinawa (OKI), Kanoya (KNY), Kakioka (KAK), and Memambetsu (MMB), respectively.

Table 1. Summary of base magnetic field values and parameters for the GS24 and GB25 cruises using reference data from the Okinawa (OKI), Kanoya (KNY), Kakioka (KAK), and Memambetsu (MMB) observatories. The definitions of each parameter are described in the Methods and Data Processing Sections. Vector components are listed in the order X (North), Y (East), and Z (Down) from top to bottom.

	GS24 cruise				GB25 cruise			
Station	OKI	KNY	KAK	MMB	OKI	KNY	KAK	MMB
T_{base} [nT]	45028.0	46848.0	46903.0	50137.0	45059.0	46878.7	46933.8	50174.5
$\mathbf{B_{base}}$ [nT]	34887.4 -3478.3 28257.2	32521.0 -4107.0 33470.0	29826.0 -4156.0 35958.0	25879.0 -4245.0 42731.0	34882.8 -3506.6 28308.8	32512.0 -4137.0 33516.2	29826.0 -4186.0 35996.4	25876.0 -4264.0 42775.4
$\mathbf{K}$	-0.0253 0.1531 0.3709	0.0447 0.0763 -0.1127	0.1271 0.2794 -0.4237	0.2556 0.2458 -1.0763	-0.0012 -0.4634 -0.5895	0.1378 -0.4647 -0.7753	0.2569 -0.7411 -0.9085	0.3125 -0.8104 -2.1889
C [nT]	-34.2207	-28.1544	-23.7764	-17.3404	-9.7058	-8.3382	-8.9081	12.3059
SD [nT]	122.9364	122.5817	122.3616	122.3327	53.0234	52.9225	52.7902	52.4698
$\mathbf{K_{IGRF}}(t_0, \mathbf{x}_0)$	-0.1045 -0.0121 0.1092	-0.0239 -0.0017 0.0223	0.0344 -0.0008 -0.0300	0.1541 -0.0047 -0.1156	0.0072 -0.0004 -0.0090	0.0878 0.0101 -0.0958	0.1459 0.0110 -0.1478	0.2656 0.0068 -0.2333
$\Delta\theta(t_0, \mathbf{x}_0)$ [°]	8.70	1.88	2.62	11.06	0.66	7.47	11.94	20.37

659

Supplementary Files

This is a list of supplementary files associated with this preprint. Click to download.

- graphicalabst.png